

Article

A Reflection-Type Dual-Band Phase Shifter with an Independently Tunable Phase

Suyeon Kim ¹ , Junhyung Jeong ², Girdhari Chaudhary ¹ and Yongchae Jeong ^{1,*}

¹ Division of Electronics and Information Engineering, Jeonbuk National University, Jeonju-si 54896, Korea; ssoo0911@jbnu.ac.kr (S.K.); girdharic@jbnu.ac.kr (G.C.)

² IT Application Research Center, Jeonbuk Regional Branch, Korea Electronics Technology Institute, Jeonju-si 54853, Korea; jjunh05@keti.re.kr

* Correspondence: ycjeong@jbnu.ac.kr

Abstract: This paper presents a design for a dual-band tunable phase shifter (PS) with independently controllable phase shifting between each operating frequency band. The proposed PS consists of a 3-dB hybrid coupler, in which the coupled and through ports terminate with the same two reflection loads. Each reflection load consists of a series of quarter-wavelength ($\lambda/4$) transmission lines, $\lambda/4$ shunt open stubs, and compensation elements at each operating frequency arm. In this design, a wide phase shifting range (PSR) is achievable at each operating frequency band (f_L : lower frequency; f_H : higher frequency) by compensating for the susceptance occurring at the co-operating frequency band caused by the $\lambda/4$ shunt open stub. The load of f_L does not affect the load of f_H and vice versa. The dual-band tunable PS was fabricated at $f_L = 1.88$ GHz and $f_H = 2.44$ GHz, and testing revealed that achieved a PSR of 114.1° with an in-band phase deviation (PD) of $\pm 8.43^\circ$ at f_L and a PSR of $114.0^\circ \pm 5.409^\circ$ at f_H over a 100 MHz bandwidth. In addition, the maximum insertion losses were smaller than 1.86 dB and 1.89 dB, while return losses were higher than 17.2 dB and 16.7 dB within each respective operating band.



Citation: Kim, S.; Jeong, J.; Chaudhary, G.; Jeong, Y. A Reflection-Type Dual-Band Phase Shifter with an Independently Tunable Phase. *Appl. Sci.* **2022**, *12*, 492. <https://doi.org/10.3390/app12010492>

Academic Editor: Ernesto Limiti

Received: 19 November 2021

Accepted: 29 December 2021

Published: 4 January 2022

Publisher's Note: MDPI stays neutral with regard to jurisdictional claims in published maps and institutional affiliations.



Copyright: © 2022 by the authors. Licensee MDPI, Basel, Switzerland. This article is an open access article distributed under the terms and conditions of the Creative Commons Attribution (CC BY) license (<https://creativecommons.org/licenses/by/4.0/>).

Keywords: dual band; phase deviation (PD); phase shifting range (PSR); reflection type; transmission line; tunable phase shifter (PS)

1. Introduction

The phase shifter (PS) is one of the most important elements in wireless communication systems, as it is widely used in beam-forming, phased array, harmonic distortion, and multiple-input multiple-output (MIMO) systems [1–8]. Tunable PSs are used with along/digital attenuators in phased array beam-forming networks where insertion loss (IL) and phase deviation (PD) must be as small as possible to steer the lobes and nulls of antennas. Tunable PSs are classified as transmission type [9,10] and reflection type [11–20]. Reflection-type PSs can provide continuous phase shift, as well as excellent return loss (RL) due to their use of a 3-dB hybrid coupler and identical reflection loads at the coupler's through and coupled ports. Since the DC power consumption of a varactor diode is much smaller than that of a PIN diode or a microwave FET, varactor diodes are widely used in PSs.

In [13], a PS with wide PSR was presented using L-type and π -type circuits, which provided a PSR of 201° for L-type and a PSR of 385° for π -type. Similarly, a reflection-type tunable PS using an impedance transforming quadrature coupler was presented in [14], in which a PSR of 234° was achieved at the center frequency. In [15], modifying the structure of [14] to cascading structure resulted in a PSR of up to 407° . A compact tunable PS which achieved a PSR of 407° was presented in [16] using a vertical planar structure. Likewise, a tunable reflection-type PS at X-band was presented in [17] using a coupled line. This PS achieved a PSR of 392° with an IL of 2.1 ± 1.3 dB over the operating band. However, the in-band maximum RL was always smaller than 10 dB. A wideband tunable PS based on a

coupled line was demonstrated in [18,19]. The coupled line compensated for the parasitic elements of the varactor diode, resulting in a wide PSR with small in-band PD and IL error across an extensive bandwidth. By using the series-shunt matching technique in a reflection-type PS, a wide PSR with minimum IL was achieved in [18].

Multi-band RF circuits and systems have recently been in the spotlight. The multiple functions they perform are the key to next-generation wireless communication, sensing, and radar applications. Such multi-functional systems are designed to operate concurrently across multiple frequency bands. However, the traditional PSs can operate only on a single band. It is more effective to implement a multi-band PSs rather than rely on multiple single-band PSs. In [21], the PS operating in dual-band was present. However, in this paper, there is no tunable characteristic, and there is a disadvantage that only an arbitrary phase difference is implemented. A dual-band 90° PS using band-pass and band-stop designs was presented in [22]. Similarly, a dual-band PS that combined two single-band PSs was developed in [23]. In [24], a multi-band PS was included a distributed amplifier for loss compensation and an LC network for compact chip size. Likewise, a dual-band PS using a two-stage dual-branch phase tuning network topology was demonstrated in [25]. However, none of these previously developed conventional dual-band PSs possess an independent controllable phase shift at each operating frequency, except the PSs proposed in [25].

In this paper, a dual-band reflection-type tunable PS is presented, in which the phase shifts at the lower frequency band (f_L) and the higher frequency band (f_H) can be independently tuned. As an experimental demonstration, the proposed PS was designed and fabricated for a f_L of 1.88 GHz and f_H of 2.44 GHz. The design was ultimately confirmed to provide a PSR of 114° in each band.

2. Design Method of Proposed Dual-Band Phase Shifter

Figure 1 depicts the proposed structure of the dual-band tunable PS, which consists of a 3-dB hybrid coupler, where the coupled and through ports terminated in the same two reflection loads. Figure 1b shows the one-port reflection load (Γ_L) that consists of a f_L operating arm and a f_H operating arm. Each arm has series transmission lines (TLs) with characteristic impedance (Z_{H0} or Z_{L0}) and electrical length (θ_{H0} or θ_{L0}), shunt open stubs with characteristic impedance (Z_{Hs} or Z_{Ls}) and electrical length (θ_{Hs} or θ_{Ls}), parasitic compensation element (L_c and C_c), and varactor diodes (C_v). The series TL and shunt open stub is $\lambda/4$ at f_L in case of f_H operating arm, and vice versa. The $\lambda/4$ shunt open stub provides a short-circuited condition at node A/node B at the co-operating frequency.

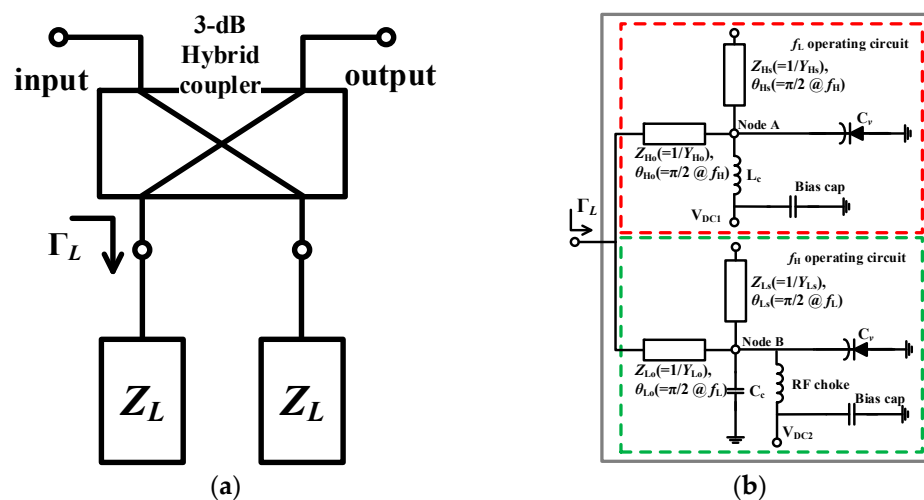


Figure 1. Structure of the proposed dual-band PS: (a) Overall two-port circuit using a 3-dB hybrid coupler and reflection loads; (b) One-port reflection load.

The series $\lambda/4$ TL transforms the short-circuited condition into an open-circuited condition at the co-operating frequency. Accordingly, the f_L and f_H operating arms imitate an open-circuited condition at f_H and f_L , respectively.

2.1. Parasitic Susceptance Compensation

Each $\lambda/4$ shunt open stub works a short-circuited condition at node A for the co-operating band. However, the $\lambda/4$ shunt open stub acts as an additional susceptance at the operating band, which affects the PSR at the operating band. Therefore, the additional susceptance at the operating band should be compensated to achieve a wide PSR.

2.1.1. Susceptance Compensation at Low-Band Operation

In the f_L operation, the co-operating band can be represented by f_H . A $\lambda/4$ shunt open stub for f_H will provide a short-circuited condition at node A. However, a $\lambda/4$ shunt open stub will act as a capacitive component at f_L because $f_L < f_H$. To compensate for this additional susceptance, the shunt inductor (L_c) is connected at node A, as shown in Figure 2a. The input admittances of the $\lambda/4$ shunt open stub and L_c when observed from node A can be expressed as (1) and (2):

$$Y_{inA}^{stub} = jY_{Hs} \tan\left(\frac{\pi f_L}{2f_H}\right) \tag{1}$$

$$Y_{inA}^{inductor} = \frac{1}{j2\pi f_L L_c} \tag{2}$$

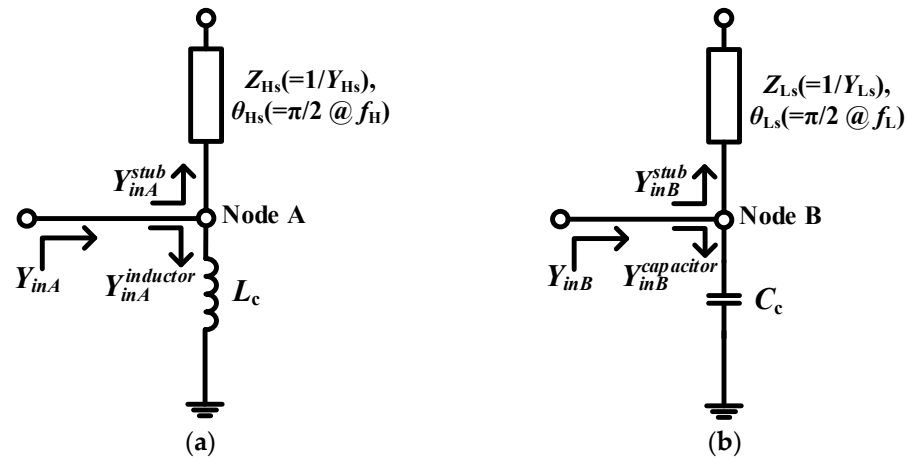


Figure 2. Compensation method according to operating band: (a) Low-band operation; (b) High-band operation.

To compensate for the parasitic effect of a $\lambda/4$ shunt open stub, Equations (1) and (2) must be conjugated. The required L_c is calculated using Equation (3):

$$L_c = \frac{1}{2\pi f_L Y_{Hs} \tan\left(\frac{\pi f_L}{2f_H}\right)} \tag{3}$$

2.1.2. Susceptance Compensation at High-Band Operation

Likewise, in an f_H operation, the co-operating band can be represented by f_L . The $\lambda/4$ shunt open stub for f_L provides a short-circuited condition at node B. However, a $\lambda/4$ shunt open stub will act as an inductive component at f_H because $f_H > f_L$. The capacitor was therefore connected in parallel to compensate the effect of the $\lambda/4$ shunt open stub, as

shown in Figure 2b. The input admittances of the $\lambda/4$ shunt open stub and shunt capacitor (C_c) from the perspective of node B can be expressed using Equations (4) and (5):

$$Y_{inB}^{stub} = jY_{Ls} \tan\left(\frac{\pi f_H}{2f_L}\right) \quad (4)$$

$$Y_{inB}^{capacitor} = j2\pi f_H C_c \quad (5)$$

The parasitic compensating C_c is given as (6):

$$C_c = -\frac{Y_{Ls} \tan\left(\frac{\pi f_H}{2f_L}\right)}{2\pi f_H} \quad (6)$$

2.2. Analysis of Phase Shifting Range

Figure 3 shows the equivalent circuits at f_L and f_H . With the exception of the series TL, none of the elements affect the PSR. By compensating for the parasitic effects of $\lambda/4$ shunt open stubs using (3) and (6), the proposed dual-band PS can achieve a PSR nearly identical to that obtained when a single alone varactor diode is used. The following sections discuss PSRs in each operating band.

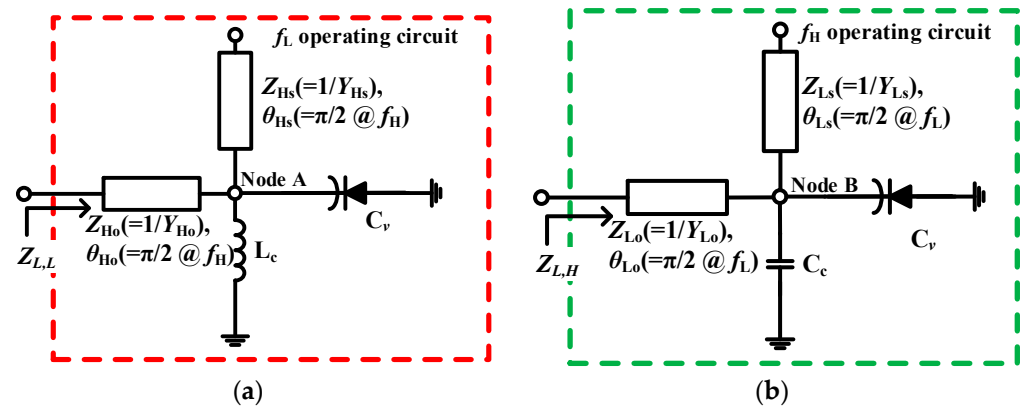


Figure 3. Each reflection load according to operating band: (a) Low-band operation; (b) High-band operation.

2.2.1. Phase Shifting Range at Low-Band Operation

During f_L operation, the L_c is used to compensate for the unwanted effect of a $\lambda/4$ shunt open stub, as shown Figure 3a. The reflection load of the circuit at f_L ($\Gamma_L^{f_L}$) can be determined using Equation (7):

$$\Gamma_L^{f_L} = \frac{-X_A Z_0 + jX_B Z_{H0}}{X_A Z_0 + jX_B Z_{H0}}, \quad (7)$$

in which:

$$X_A = Z_{H0} Z_{Hs} \cot \theta_{Hs} - \omega L_c Z_{H0} - \omega L_c Z_{Hs} - \omega^2 C_v L_c Z_{H0} Z_{Hs} \cot \theta_{Hs} \quad (8a)$$

$$X_B = Z_{H0} Z_{Hs} + \omega L_c Z_{Hs} \cot \theta_{Hs} - \omega L_c Z_{H0} \tan \theta_{H0} - \omega^2 C_v L_c Z_{H0} Z_{Hs} \quad (8b)$$

$$\theta_{Hs} = \frac{\pi f}{2f_H}, \theta_{H0} = \frac{\pi f}{2f_L} \quad (8c)$$

and f is an operating frequency. From (7), the magnitude and phase of $\Gamma_L^{f_L}$ are determined using Equation (9a,b):

$$|\Gamma_L^{f_L}| = 1 \quad (9a)$$

$$\angle \Gamma_L^{f_L} = \phi_{f_L} = \pi - 2 \tan^{-1} \left(\frac{X_B Z_{H0}}{X_A Z_0} \right) \tag{9b}$$

Using (9b), the PSR of the proposed structure at f_L can be expressed as the result of Equation (10), in which subscript V represents the bias voltage that changes the capacitance of C_v by varying V_{min} to V_{max} :

$$\Delta \phi_{f_L} \Big|_V = \begin{cases} \phi_{f_L} \Big|_V - \phi_{f_L} \Big|_{V_{min}} & \text{if } \phi_{f_L} \Big|_{V_{min}} < \phi_{f_L} \Big|_{V_{max}} \\ \phi_{f_L} \Big|_V - \phi_{f_L} \Big|_{V_{max}} & \text{if } \phi_{f_L} \Big|_{V_{min}} > \phi_{f_L} \Big|_{V_{max}} \end{cases} \tag{10}$$

Table 1 shows the calculated values of PSR and PD according to Z_{H0} and Z_{Hs} . For demonstrations, $f_L = 1.88$ GHz, $f_H = 2.44$ GHz, and BW was 100 MHz. The value of L_c was calculated using (3), while C_v was implemented using a SMV-1231 from SKYWORKS, which provided variable capacitance by varying the bias voltage from 0 V to 16 V. PSR and PD at the f_L band increased along with Z_{H0} . The PSR of the f_L band was remained constant, even though Z_{Hs} increased. However, the PD of the f_L band decreased and the PD of the f_H band increased as Z_{Hs} increased. These results highlight that an appropriate Z_{H0} and Z_{Hs} must be selected to achieve the desired PSR and PD depending on the requirements of a specific application.

Table 1. Calculated PSR and in-band PD with Z_{H0} , Z_{Hs} , and C_v .

Z_{H0} [Ω]	Z_{Hs} [Ω]	PSR [$^\circ$] (f_L/f_H)	PD [$^\circ$] (f_L/f_H)
30		56.3/0	$\pm 1.19/\pm 3.04$
40		84.21/0	$\pm 4.69/\pm 2.15$
50	120	107.74/0	$\pm 10.69/\pm 1.4$
60		124.9/0	$\pm 18.45/\pm 0.98$
70		136.31/0	$\pm 27.22/\pm 0.72$
	100	107.74/0	$\pm 13.07/\pm 0.92$
	110	107.74/0	$\pm 11.77/\pm 1.14$
50	120	107.74/0	$\pm 10.69/\pm 1.4$
	130	107.74/0	$\pm 9.76/\pm 1.69$
	140	107.74/0	$\pm 8.97/\pm 2.01$

The design goals were specified as PSR > 100° at the f_L band, PD < 15° at the f_L band, and PD < 1.5° at the f_H band. For these specified design goals, the circuit parameters selected were $Z_{H0} = 50 \Omega$ and $Z_{Hs} = 120 \Omega$. Figure 4 shows the calculated PSR according to C_v variation.

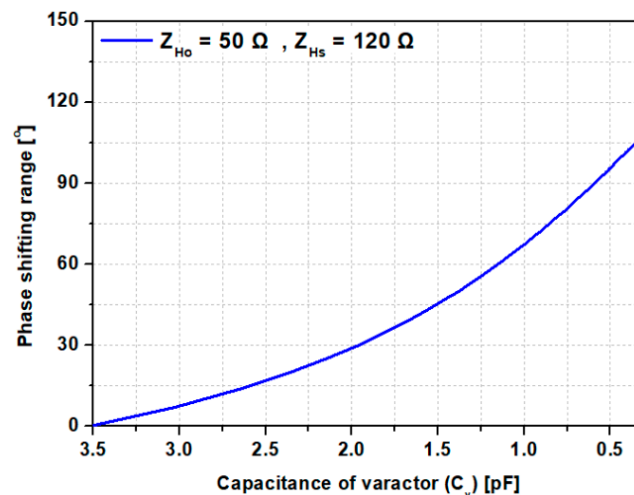


Figure 4. PSR with C_v variations at f_L ($C_v = 3.5$ to 0.3 pF @ f_L).

Figure 5 depicts the PSR with and without compensation of for the $\lambda/4$ shunt open stub. The proposed PS achieved a PSR of 114° at the f_L band when the effect of the $\lambda/4$ shunt open stub was compensated for. However, PSR was reduced to 40° in cases where compensation was absent.

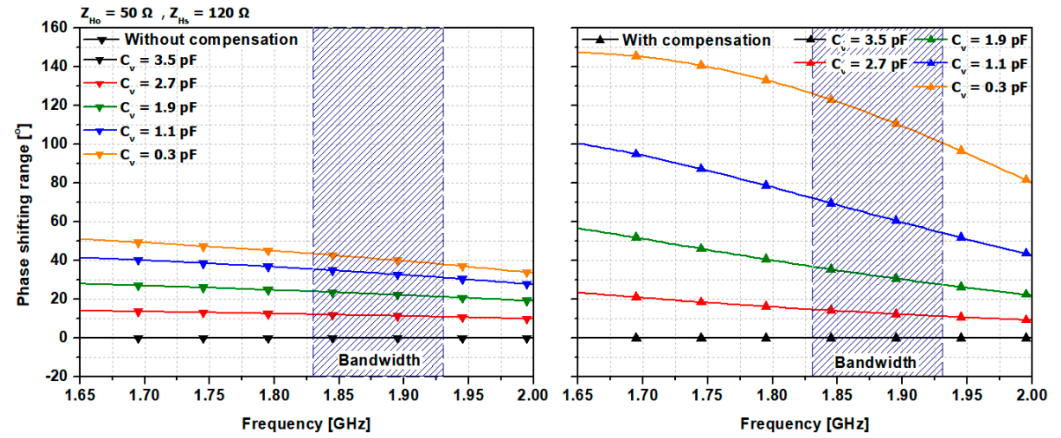


Figure 5. PSR with and without compensating for the effects of a $\lambda/4$ shunt open stub at the low-band.

2.2.2. Phase Shifting Range at High-Band Operation

During f_H operation, the unwanted effect of a $\lambda/4$ shunt open stub was compensated by C_c , as shown in Figure 3b. The reflection load at f_H ($\Gamma_L^{f_H}$) is determined using Equation (11):

$$\Gamma_L^{f_H} = \frac{-X_C Z_0 + jX_D Z_{L_0}}{X_C Z_0 + jX_D Z_{L_0}}, \tag{11}$$

in which:

$$X_C = Z_{L_0} + Z_{L_S} \cot \theta_{L_S} + 2\pi f(C_v + C_c)Z_{L_0}Z_{L_S} \cot \theta_{L_S} \tag{12a}$$

$$X_D = Z_{L_0} \tan \theta_{L_0} - Z_{L_S} \cot \theta_{L_S} + 2\pi f(C_v + C_c)Z_{L_0}Z_{L_S} \tag{12b}$$

$$\theta_{L_S} = \frac{\pi f}{2f_L}, \theta_{L_0} = \frac{\pi f}{2f_L} \tag{12c}$$

From (12), the magnitude and phase of $\Gamma_L^{f_H}$ can be determined using (13):

$$|\Gamma_L^{f_H}| = 1 \tag{13a}$$

$$\angle \Gamma_L^{f_H} = \phi_{f_H} = \pi - 2 \tan^{-1} \left(\frac{X_D Z_{L_0}}{X_C Z_0} \right) \tag{13b}$$

Using (13b), the PSR of the proposed structure can be expressed using Equation (14), in which subscript V represents a bias voltage of varactor:

$$\Delta \phi_{f_H} \Big|_V = \begin{cases} \phi_{f_H} \Big|_V - \phi_{f_H} \Big|_{V_{\min}} & \text{if } \phi_{f_H} \Big|_{V_{\min}} < \phi_{f_H} \Big|_{V_{\max}} \\ \phi_{f_H} \Big|_V - \phi_{f_H} \Big|_{V_{\max}} & \text{if } \phi_{f_H} \Big|_{V_{\min}} > \phi_{f_H} \Big|_{V_{\max}} \end{cases} \tag{14}$$

Table 2 shows that the calculated PSR and PD values as Z_{L_0} and Z_{L_S} varied. Consistent with f_L band operation, $f_L = 1.88$ GHz, $f_H = 2.44$ GHz, and BW was 100 MHz. The value of C_c that compensated for the effect of a $\lambda/4$ shunt open stub was calculated using (6), while C_v was implemented using a varactor SMV-1231 from SKYWORKS, which provided a variable capacitance of 4.7 pF to 0.3 pF by varying the bias voltage from 0 V to 16 V. The PSR at the f_H band decreased as Z_{L_0} increased, however, PD at the f_H band increased. Similarly, PSR remained constant as Z_{L_S} increased. PD, however, increased at the f_L band

while PD decreased at the f_H band. Therefore, appropriate Z_{L_o} and Z_{L_s} values should be selected to achieve the desired PSR and PD, keeping in mind the specific application.

Table 2. Calculated PSR and in-band PD with Z_{L_o} , Z_{L_s} , and C_v .

Z_{L_o} [Ω]	Z_{L_s} [Ω]	PSR [$^\circ$] (f_L/f_H)	PD [$^\circ$] (f_L/f_H)
30	120	0/141.08	4.11/4.93
40		0/135.7	2.55/4.55
50		0/121.82	1.68/9.30
60		0/106.67	1.18/12.75
70		0/92.58	0.87/14.58
50	100	0/121.82	1.11/11.36
	110	0/121.82	1.38/10.24
	120	0/121.82	1.68/9.30
	130	0/121.82	2.02/8.51
	140	0/121.82	2.39/7.83

Like the f_L operation, the design goals were specified as PSR > 100° at the f_H band and PD < 2° and 10° at the f_L and f_H band, respectively. To achieve these design goals, the circuit parameters were selected as $Z_{L_o} = 50 \Omega$ and $Z_{L_s} = 120 \Omega$. Figure 6 shows the calculated PSR according to C_v variations.

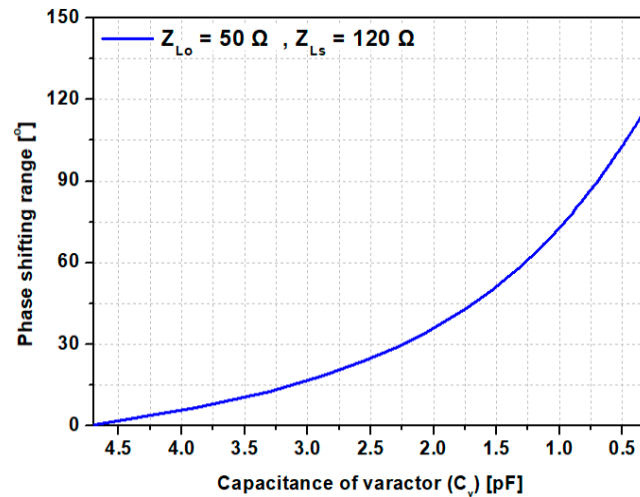


Figure 6. PSR with C_v variations at f_H ($C_v = 4.7$ to 0.3 pF @ f_H).

Figure 7 depicts the PSR with and without compensation for the $\lambda/4$ shunt open stub. A PSR of 116° at the f_H band was achieved with compensation. However, the PSR increased to 203° in the absence of compensation. In the event that a wider PSR was desired, a circuit lacking compensation would be appropriate. We, however, assessed a circuit with compensation in order to obtain the same PSR as the varactor diode.

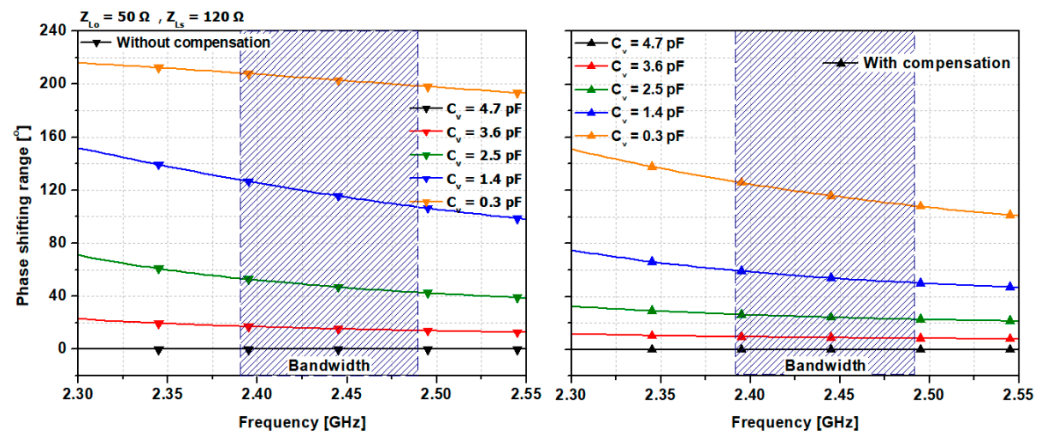


Figure 7. PSR with and without compensating for the effects of a $\lambda/4$ shunt open stub at the high band.

3. Simulation and Measurement Results

The proposed dual-band tunable PS was designed and fabricated at $f_L = 1.88$ GHz and $f_H = 2.44$ GHz with an operating bandwidth of 100 MHz, using a substrate RT/Duroid 5880 with a dielectric constant (ϵ_r) of 2.2 and a thickness (h) of 0.787 mm. The simulation was performed by using advanced design system (ADS) simulator. The variable capacitance C_V was implemented using a varactor diode SMV-1231 from SKYWORKS. A 3-dB hybrid coupler S03A2500N1 from ANAREN was also used. Figure 8 shows a layout and photograph of the designed dual-band tunable PS.

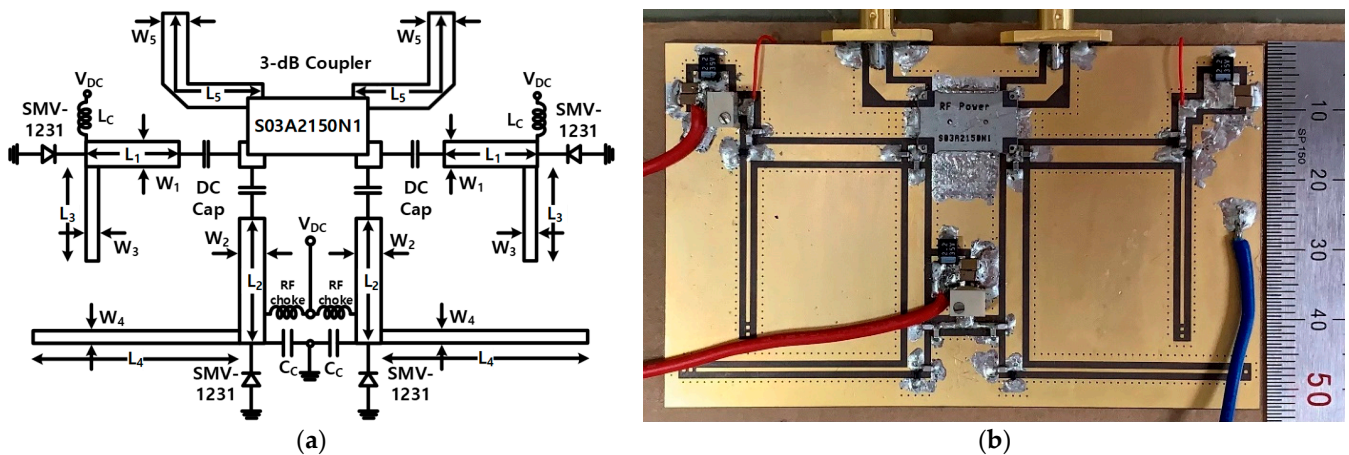


Figure 8. (a) Layout and (b) photograph of fabricated dual-band tunable reflection-type PS.

Figure 8a defines the transmission line width, length, and components in the entire circuit, and their values are listed in Table 3. The part number and measured value of DC block capacitor, RF choke inductor, bypass capacitor, L_C , and C_C at f_L and f_H are also listed. The overall size of the fabricated circuit was 85 mm \times 52 mm.

Table 3. Physical dimensions and component value of fabricated PCB.

$W_1 = W_2 = W_5 = 2.4$ mm	$W_3 = W_4 = 0.5$ mm	$L_1 = 22$ mm
$L_2 = 29$ mm	$L_3 = 23$ mm	$L_4 = 30$ mm
$L_5 = 13.6$ mm	$L_C = 5R4 15R4$ (Part no.)/3.82 pF (@ f_H)	$C_C = 0R8$ (Part no.)/1 pF (@ f_L)
DC block capacitor: 120 J	RF choke inductor: 3R9	Bypass capacitor: 8R2
56.6 pF (@ f_L)/216 pH (@ f_H)	76.02 nH (@ f_L)/223.8 nH (@ f_H)	12 pF (@ f_L)/29.01 pF (@ f_H)

3.1. Results of Low-Band Operation

Figure 9 presents out simulated and measured results achieved by varying the bias voltage of the varactor diode in the f_L band and fixing the bias voltage to 0 V in the f_H band. Figure 9a shows the simulated and measured PSRs. The phase at f_L band tuned, while the f_H band was maintained constantly. Based on our experiment, we determined that the PSR of the f_L was $114.194^\circ \pm 8.2615^\circ$ within a bandwidth of 100 MHz, a result that was achieved by varying the bias voltage from 0 V to 16 V. While varying the phase at the f_L band, the phase of f_H remained at $0.225^\circ \pm 0.936^\circ$ within the bandwidth. Figure 9b shows the simulated and measured IL and input/output RLs. The measured ILs at the f_L band and the f_H band were smaller than 1.867 dB and 1.897 dB, and the input/output RLs were higher than 19.674 dB and 16.684 dB, respectively.

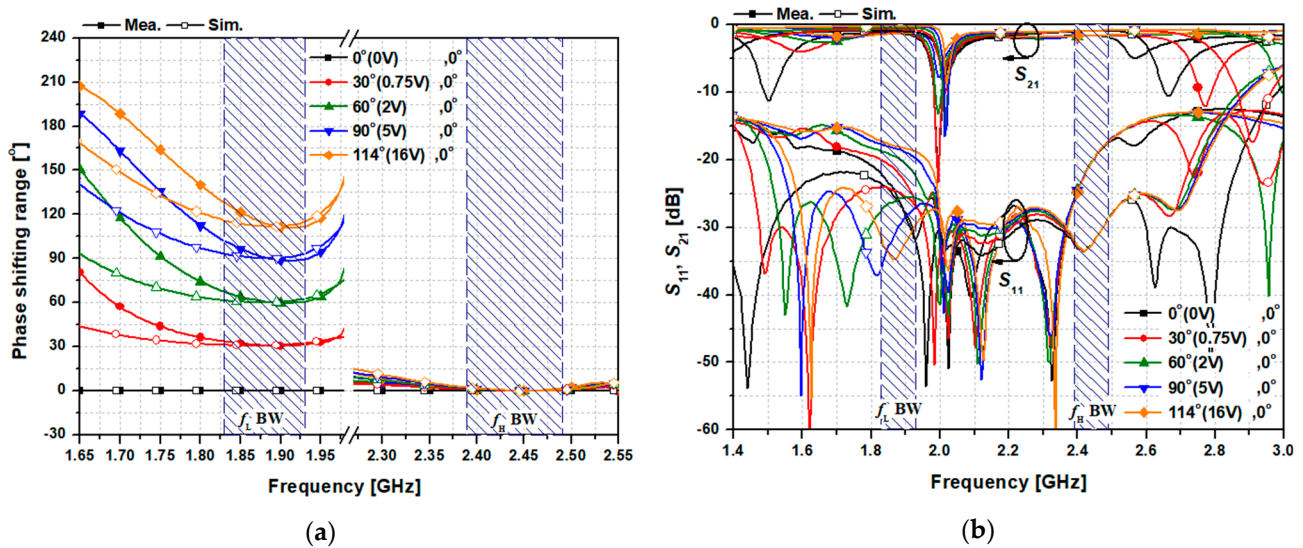


Figure 9. Simulated and measured results of a dual-band PS achieved by varying the bias voltage of the low –band while fixing the bias voltage of the high-band at 0 V: (a) PSRs; (b) ILs and input/output RLs.

Table 4 provides the measured results after varying the bias voltage of the varactor diode at the f_L band and fixing the bias voltage at 2.5 V and 16 V at the f_H band. As seen from Table 4, the f_L band achieved almost the same PSR and the phase of the f_H was constantly maintained. The measured ILs were smaller than 2 dB, and RLs were higher than 19.6 dB.

Table 4. Measured results of the dual-band PS achieved by varying the bias voltage of the low-band while fixing the bias voltage of the high-band.

Bias Voltage [V] (f_L/f_H)	PSR [°] @ f_L	Phase [°] @ f_H	PD [°] (f_L/f_H)	Max. IL [dB] (f_L/f_H)	Min. RL [dB] (f_L/f_H)
0 to 16/2.5	114.067	60	$\pm 8.396/\pm 0.342$	1.580/1.989	19.669/21.077
0 to 16/16	114.494	114	$\pm 9.465/\pm 0.667$	1.414/1.419	19.695/25.047

@: means operating center frequency.

3.2. Results of High-Band Operation

Figure 10 shows the simulated and measured results of the dual-band PS achieved by varying the f_H band bias voltage from 0 V to 16 V and fixing the bias voltage at 0 V in the f_L band. The PSR of the f_H band was $114.097^\circ \pm 6.076^\circ$, and the phase at the f_L band was maintained at $0.360^\circ \pm 1.035^\circ$. The measured ILs were smaller than 1.867 dB and 1.983 dB, and RLs were higher than 22.550 dB and 16.833 dB within the two bands.

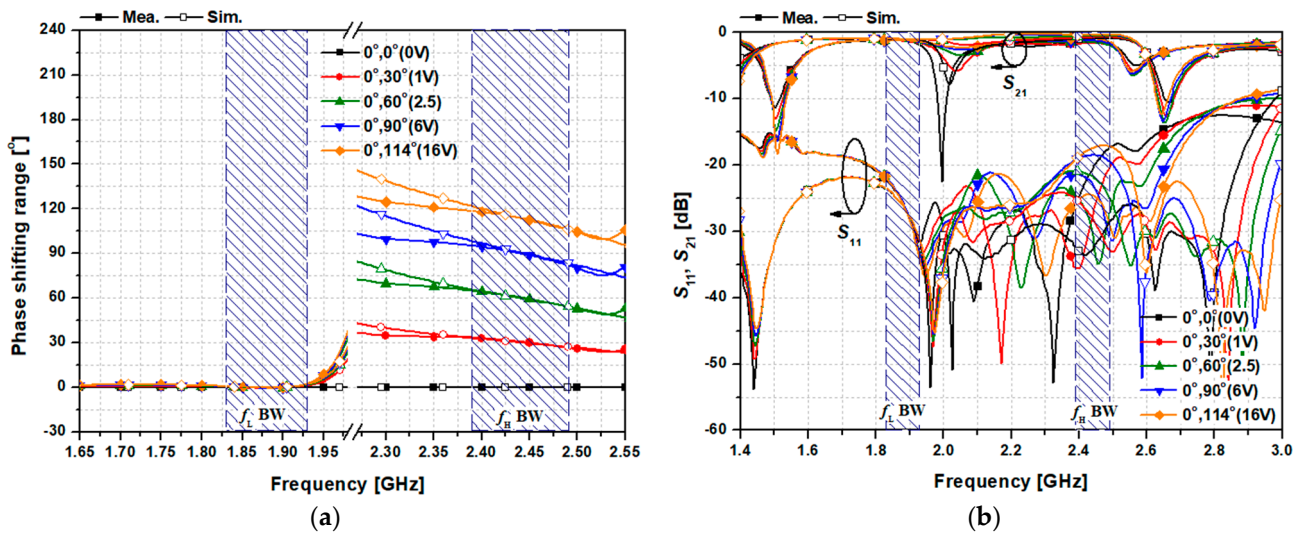


Figure 10. Simulated and measured results of a dual-band PS achieved by varying the bias voltage of the high-band while fixing the bias voltage of the low-band at 0 V: (a) PSRs; (b) ILs and input/output RLs.

Table 5 presents the measured results when the bias voltage of the varactor diode at the f_H band was varied and fixing the bias voltage was fixed at 2 V and 16 V at the f_L band. As seen from Table 5, the f_H band achieved a nearly identical PSR while the phase of the f_L was constantly maintained. The measured ILs were smaller than 1.9 dB, and RLs were higher than 16.7 dB.

Table 5. Measured results of the dual-band PS achieved by varying the bias voltage of the high-band while fixing the bias voltage of the low-band.

Bias Voltage [V] (f_L/f_H)	Phase [°] @ f_L	PSR [°] @ f_H	PD [°] (f_L/f_H)	Max. IL [dB] (f_L/f_H)	Min. RL [dB] (f_L/f_H)
2/0 to 16	60	113.947	$\pm 1.035/\pm 5.555$	1.485/1.851	20.670/16.710
16/0 to 16	114	114.242	$\pm 0.168/\pm 5.897$	1.514/1.735	19.662/16.724

@: means operating center frequency.

3.3. Simultaneous Dual-Band Operating Results

Figure 11 shows the simulated and measured results of the dual-band PS in the circumstance where the bias voltages of the f_L and f_H bands were simultaneously shifted. As seen in Figure 11a, the PSRs of the f_L and f_H bands were $114.134^\circ \pm 8.43^\circ$ and $114.017^\circ \pm 5.409^\circ$ within the bandwidth, a result achieved by varying the bias voltage from 0 V to 16 V. The ILs were smaller than 1.867 dB and 1.897 dB, and the input/output RLs were higher than 19.695 dB and 16.833 dB within bandwidth of the f_L and f_H bands.

A comparison of the performance of the proposed dual-band PS against previously reported PSs is provided in Table 6. Although the previous PSs perform very well, in as much as they achieve a wide PSR and low in-band PD, these designs are single-band operation only. The proposed design, in contrast, is of a dual-band PS with independently controllable phase shifts in each band. In addition, unlike previously published papers, using a transmission line with an electrical length of $\lambda/4$ without a band-pass filter or a band-stop filter has the advantage of being able to fabricate more easily without using a compound process and can operate independently without affecting the co-operating frequency. This proposed design had a higher RLs, lower in-band PDs, and used fewer varactor diodes than previous PSs.

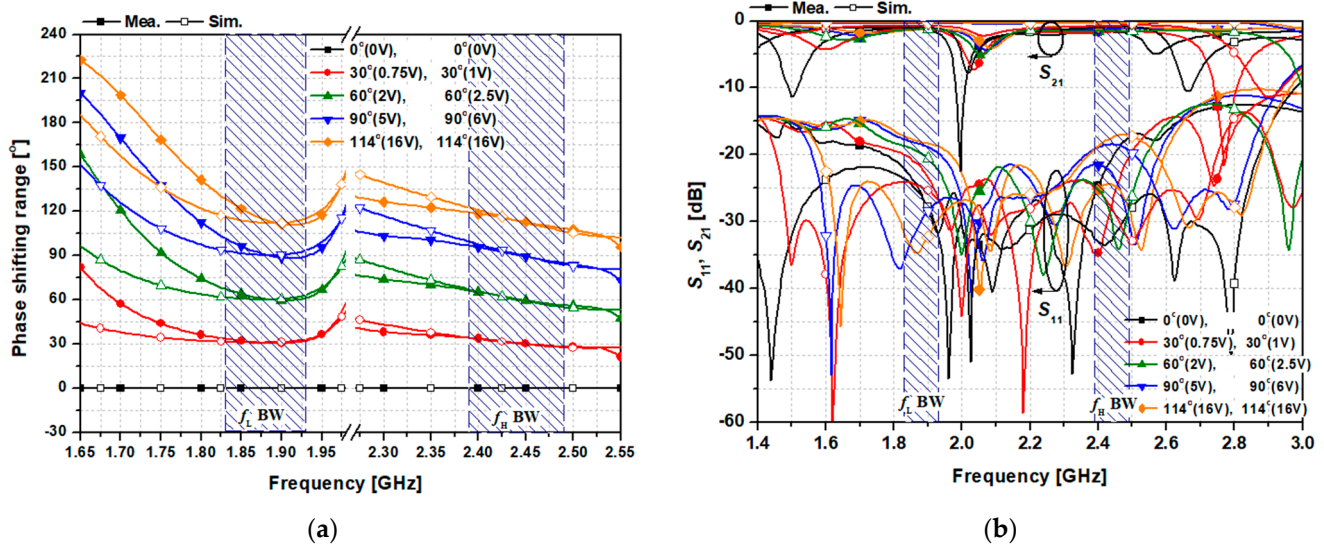


Figure 11. Simulated and measured results of a dual-band PS achieved by simultaneously varying the bias voltages of the low- and high-band: (a) PSR; (b) ILs and input/output RLs.

Table 6. Performance of the proposed design against state-of-art alternatives.

References	Freq. [GHz]	BW [GHz]	Number of Varactors	IL [dB]	RL [dB]	PSR [°]	PD [°]	Dual-Band	Size [mm × mm]
[13]	2	0.2	6	<1.56	>13.4	385	NA	X	81 × 117
[14]	2	0.2	2	<4.6	>12	234	NA	X	49 × 51
[15]	2	0.2	4	<4.6	>14	407	NA	X	69 × 51
[16]	1.5	1	4	<5.8	>14	350	±100	X	52 × 32
[17]	10	2	4	<3.4	>10	392	NA	X	NA
[18]	2.2	0.8	2	<3.2	>10	360	±15	X	19.4 × 17
[19]	2.5	0.5	4	<1.28	>15.76	146.9	±5.79	X	NA
[20]	10	2	2	<2.3	>10	190	±10	X	NA
[24]	3.5	0.02	NA	<3.7	>10	360	±3	Yes	2.3 × 1.2 (IBM 180-nM RF CMOS)
[25]	5.9	0.2	12	<2.8	>10	106	NA/±7	Yes (independently)	0.92 × 1.06 (0.25 um GaAs process)
This work	1.88 2.44	0.1 0.1	4	<1.867 <1.897	>19.695 >16.833	114.1 114.0	±8.43 ±5.40	Yes (independently)	85 × 52

4. Conclusions

This paper presents an independently controllable dual-band tunable reflection-type PS. The proposed dual-band PS uses compensation elements to deal with the unwanted parasitic elements of a co-operating band with a shunt open stub and achieves wide PSRs at two operating bands. In the event that the ratio of two operating frequencies is greater than two and less than three, the inductor could be used as the same compensation element for both operating bands. The proposed dual-band PS was verified by fabricating the circuit at 1.88 GHz and 2.44 GHz. Furthermore, the proposed dual-band PS is easy to manufacture and would be useable in a number of diverse dual-band RF circuits and systems.

Author Contributions: Conceptualization, J.J. and Y.J.; methodology, S.K. and G.C.; software, S.K.; validation, G.C. and Y.J.; formal analysis, S.K. and G.C.; investigation, S.K.; resources, Y.J.; data curation, S.K.; writing—original draft preparation, S.K.; writing—review and editing, S.K., G.C. and Y.J.; visualization, S.K.; supervision, Y.J.; project administration, Y.J.; funding acquisition, Y.J. All authors have read and agreed to the published version of the manuscript.

Funding: This research was supported by a grant from the National Research Foundation (NRF) of Korea funded by the Korean Government (MSIT) (No. 2020R1A2C2012057) and by a grant from the Basic Science Research Program, administered through the NRF and funded by the Ministry of Education (No. 2019R1A6A1A09031717).

Institutional Review Board Statement: Not applicable.

Informed Consent Statement: Not applicable.

Data Availability Statement: Not applicable.

Conflicts of Interest: The authors declare that they have no conflicts of interest to report regarding the present study.

References

- De Luis, J.R.; De Flaviis, F. A reconfigurable dual frequency switched beam antenna array and phase shifter using PIN diodes. In Proceedings of the IEEE Antennas and Propagation Society International Symposium, North Charleston, SC, USA, 1–5 June 2009.
- Wang, W.; Chen, C.; Wang, S.; Wu, W. Switchable dual-band dual-sense circularly polarized patch antenna implemented by dual-band phase shifter of $\pm 90^\circ$. *IEEE Trans. Antennas Propag.* **2021**, *69*, 6912–6917. [[CrossRef](#)]
- Shiroma, G.S.; Miyamoto, R.Y.; Shiroma, W.A. A full-duplex dual-frequency self-steering array using phase detection and phase shifting. *IEEE Trans. Microw. Theory Tech.* **2006**, *54*, 128–134. [[CrossRef](#)]
- Sobhy, E.A.; Hoyos, S. A multiphase multipath technique with digital phase shifters for harmonic distortion cancellation. *IEEE Trans. Circuits Syst. II Exp. Briefs.* **2010**, *57*, 921–925. [[CrossRef](#)]
- Szortyka, V.; Raczkowski, K.; Kuijk, M.; Wambacq, P. A wideband beamforming lowpass filter for 60 GHz phased-array receivers. *IEEE Trans. Circuits Syst. I Reg. Pap.* **2015**, *62*, 2324–2333. [[CrossRef](#)]
- Yang, X.; Lin, J. A digitally controlled constant envelop phase-shift modulator for low-power broadband wireless applications. *IEEE Trans. Microw. Theory Tech.* **2006**, *54*, 96–105. [[CrossRef](#)]
- Gatti, R.V.; Ocera, A.; Marcaccioli, L.; Sorrentino, R. A dual band reconfigurable power divider for WLAN applications. In Proceedings of the IEEE MTT-S International Microwave Symposium Digest, San Francisco, CA, USA, 11–16 June 2006.
- Öjefors, E.; Cheng, S.; From, K.; Skarin, I.; Hallbjörner, P.; Rydberg, A. Electrically steerable single-layer microstrip traveling wave antenna with varactor diode-based phase shifters. *IEEE Trans. Antennas Propag.* **2007**, *55*, 2451–2460. [[CrossRef](#)]
- LaRocca, T.; Tam, S.W.; Hyang, D.; Gu, Q.; Socher, E.; Hant, W.; Chang, F. Millimeter-wave CMOS digital controlled artificial dielectric transmission lines for reconfigurable ICs. In Proceedings of the IEEE MTT-S International Microwave Symposium Digest, Atlanta, GA, USA, 15–20 June 2008.
- Woods, W.H.; Valdes-Garcia, A.; Ding, H.; Rascoe, J. CMOS millimeter wave phase shifter based on tunable transmission lines. In Proceedings of the IEEE Custom Integrated Circuits Conference, San Jose, CA, USA, 22–25 September 2013.
- Upshur, J.I.; Geller, B.D. Low-loss 360° X-band analog phase shifter. In Proceedings of the IEEE International Digest on Microwave Symposium, Dallas, TX, USA, 8–10 May 1990.
- Liew, Y.H.; Joe, J.; Leong, M.S. A novel 360° analog phase shifter with linear voltage phase relationship. In Proceedings of the IEEE Asia-Pacific Microwave Conference, Singapore, 30 November–3 December 1999.
- Burdin, F.; Iskandar, Z.; Podevin, F.; Ferrari, P. Design of compact reflection-type phase shifters with high figure-of-merit. *IEEE Trans. Microw. Theory Tech.* **2015**, *63*, 1883–1893. [[CrossRef](#)]
- Lin, C.S.; Chang, S.F.; Chang, C.C.; Shu, Y.H. Design of a reflection-type phase shifter with wide relative phase shift and constant insertion loss. *IEEE Trans. Microw. Theory Tech.* **2007**, *55*, 1862–1868. [[CrossRef](#)]
- Lin, C.S.; Chang, S.F.; Hsiao, W.C. A full 360° RTPS with constant insertion loss. *IEEE Microw. Compon. Lett.* **2008**, *18*, 106–108.
- Liu, W.J.; Zheng, S.Y.; Pan, Y.M.; Li, Y.X.; Long, Y.L. A wideband tunable reflection-type phase shifter with wide relative phase shift. *IEEE Trans. Circuit Syst. II Exp. Briefs* **2017**, *64*, 1442–1446. [[CrossRef](#)]
- Venter, J.J.P.; Stander, T.; Ferrari, P. X-band reflection-type phase shifters using coupled-line couplers on single-layer RF PCB. *IEEE Microw. Wirel. Compon. Lett.* **2018**, *28*, 807–809. [[CrossRef](#)]
- Abbosh, M. Compact tunable reflection phase shifters using short section of coupled lines. *IEEE Trans. Microw. Theory Tech.* **2012**, *60*, 2465–2472. [[CrossRef](#)]
- An, B.; Chaudhary, G.; Jeong, Y. Wideband tunable phase shifter with low in-band phase deviation using coupled line. *IEEE Microw. Wirel. Compon. Lett.* **2018**, *28*, 678–680. [[CrossRef](#)]
- Singh, A.; Mandal, M.K. Electronically tunable reflection type phase shifters. *IEEE Trans. Circuits Syst. II Exp. Briefs* **2020**, *67*, 425–429. [[CrossRef](#)]

21. Dong, Q.; Wu, Y.; Chen, W.; Yang, Y.; Wang, W. Single-Layer Dual-Band Bandwidth-Enhanced Filtering Phase Shifter With Two Different Predetermined Phase-Shifting Values. *IEEE Trans. Circuits Syst. II Exp. Briefs* **2021**, *68*, 236–240. [[CrossRef](#)]
22. Itoh, Y.; Takagi, H. A dual-band 90-degree SiGe HBT active phase shifter using band-pass and band-stop designs. In Proceedings of the European Microwave Conference (EuMC), Nuremberg, Germany, 10–12 October 2017.
23. Banbury, D.R.; Fayyaz, N.; Safavi-Naeini, S.; Nikneshan, S. A CMOS 5.5/2.4 GHz dual-band smart-antenna transceiver with a novel RF dual-band phase shifter for WLAN 802.11a/b/g. In Proceedings of the IEEE Radio Frequency Integrated Circuits (RFIC) Systems, Digest of Papers, Forth Worth, TX, USA, 6–8 June 2004.
24. Lu, C.; Pham, A.-V.H.; Livezey, D. Development of multiband phase shifters in 180-nm RF CMOS technology with active loss compensation. *IEEE Trans. Microw. Theory Tech.* **2006**, *54*, 40–45.
25. Xiong, Y.; Zeng, X.; Li, J. A tunable concurrent dual-band phase shifter MMIC for beam steering applications. *IEEE Trans. Circuits Syst. II Exp. Briefs* **2020**, *67*, 2412–2416. [[CrossRef](#)]